Journal of
Nanomedicine & Nanotechnology

Deiwick et al., J Nanomed Nanotechnol 2014, 5:6
DOI: 10.4172/2157-7439.1000239

Research Article Open Access

Functional Titanium Lotus-Topography Promotes the Osteoinduction of Human Adipose-Derived Stem Cells *In Vitro*

Andrea Deiwick[1], Elena Fadeeva[1], Lothar Koch[1], Reiner Gebauer[1], Boris Chichkov[1,2] and Sabrina Schlie-Wolter[1,2]*

[1]*Laser Zentrum Hannover e.V.; Nanotechnology Department; Hollerithallee 8; D-30419 Hannover, Germany*
[2]*Institute of Quantum Optics; Leibniz University Hannover; Welfengarten 1; D-30167 Hannover, Germany*

Abstract

For orthopedic applications, biomaterials are required which (a) enable bone cell anchorage, (b) stimulate osteogenic differentiation, (c) reduce the risk of infections and immune rejection, and (d) have appropriate mechanical properties similar to native bone. To enhance the biological performance of titanium, surface structuring by ultrashort-pulse laser ablation was tested. This nanotechnology enables high precision, reduced head-affected zones, and small amount of debris around the ablated area. Various surface features in almost all solid materials can be fabricated. In order to mimic the complex architecture of natural bone, a lotus-topography was generated. Recently, we demonstrated that lotus-features reduce immune rejection and minimize the risk of infections *in vitro*.

Using human adipose-derived stem cells (hASC) we show that significantly more cells were adherent on the topography due to the increased surface area for contact. The distribution of integrin subunits got organized: β_1 integrins were located on the tip of the structures, α_5 integrins on the bottom. Furthermore, lotus-structures enhanced cell adhesion forces, quantified by centrifugation detachment assay. We further focused on surface impacts on osteogenic differentiation. Thereby, lotus-structures presented a strong promotive effect. Predifferentiated cells did not dedifferentiate, undifferentiated cells differentiated directly. However, differences of the tested osteogenic markers were obtained: alkaline phosphatase activity was not increased by the surface features, while osteocalcin expression and calcium mineralization, the strongest bone cell marker, were significantly improved.

In a sum, lotus-structures represent a surface functionalization which advances the functionality of titanium: namely osteoinduction and bioactivity *In vitro*. Therefore, they hold a great promise for future orthopedic applications.

Keywords: Bioactivity; Nanotechnology; Adhesion; Stem cells; Osteoinduction

Abbreviations: 3D: Three-Dimensional; ALP: Alkaline Phosphatase; BMP: Bone Morphogenic Protein; ECM: Extracellular Matrix; EDX: Energy-Dispersive X-ray Spectrometry; Eth-1: Ethidium Homodimer-1; FAK p-Tyr^{397}: Focal Adhesion Kinase; hASC: human Adipose-derived Stem Cells; LDH: Lactate Dehydrogenase; PBS: Phosphate Buffer Saline; Prediff: Predifferentiated cells; SEM: Scanning Electron Microscopy; s.e.m.: standard error of mean; Ti: Titanium

Introduction

Orthopedic implant failure is not only related to technical problems like stress shielding effects, fatigue, low wear and corrosion resistance of the material [1]. Failure is further related to biological problems: corrosion debris can be responsible for allergic and toxic reactions. Infections and immune rejection, which leads to fibrotic capsule formation and thereby isolation of the implant, often result in re-implantation [2,3]. Since the substitution of the orthopedic core material is difficult related to mechanical aspects, research has turned over to modify the implant surface, adapting it more accurately to the *in vivo* situation.

Owing to its perfect mechanical performance, which reflects a high specific strength and elastic modulus similar to native bone, titanium (Ti) is the material of choice for orthopedic and dental applications [1,4]. A thin oxide layer on its surface further supports the corrosion resistance. Even though Ti is bioinert, its bone-binding activity is pretty low compared to other materials like calcium phosphates, polymers or ceramics – but whose mechanical properties are unsatisfactory on the contrary [5]. However, this limitation of Ti negatively affects its biological performance: poor anchorage of bone decelerates bone healing and regeneration. Material functionalization strategies like specific coatings, incorporation of bioactive osteoinductive molecules with for instance bone-morphogenic proteins (BMP) or a topographical functionalization were shown to enhance Ti's capacity to bind bone and induce osseointegration [1,6,7]. Osseointegration is characterized by strong anchorage of bone cells followed by osteogenic differentiation [6]. Several markers classify such differentiation like increase in alkaline phosphatase activity (ALP), the synthesis of collagen type I matrix, and the expression of osteocalcin and osteopontin. But the strongest sign for Osseo integration is calcium phosphate deposition, which identifies functional mineralized bone matrix [8]. Therefore, osteoinductive materials have to implicate appropriate mechanical properties, strong anchorage of bone cells and calcium phosphate mineralization on their surface.

A topographical functionalization requires a reliable technology, which enables a reproducible fabrication of various surface features with controllable size dimensions of orthopedic relevant materials. Ultrashort-pulse laser ablation, a nanotechnology, fulfills these demands and owns additional benefits such as high precision, low mechanical damages of the material and no heat-affected zones. By this, various surface features in micro- and nanoscale can be fabricated and

***Corresponding author:** Sabrina Schlie-Wolter, Laser Zentrum Hannover e.V., Hollerithallee 8, 30419 Hannover, Germany, Tel: 49-511-2788-303; Fax: 49-511-2788-100; E-mail: s.schlie@lzh.de

Received September 01, 2014; **Accepted** October 17, 2014; **Published** October 25, 2014

Citation: Deiwick A, Fadeeva E, Koch L, Gebauer R, Chichkov B, et al. (2014) Functional Titanium Lotus-Topography Promotes the Osteoinduction of Human Adipose-Derived Stem Cells *In Vitro*. J Nanomed Nanotechnol 5: 239. doi: 10.4172/2157-7439.1000239

used as a platform to study systematically material-cell-interactions in a defined topographical environment [9-11]. To mimic the hierarchical architecture of native bone, a more complex surface design is needed, namely a combination of microscale structures superimposed with nano-roughness. So-called lotus-surfaces, which mimic the surface of the lotus *Nelumba lucifera* leaf, are formed spontaneously after laser irradiation on Ti, making ultrashort-pulse laser ablation very attractive for orthopedic applications [12].

We recently reported that these lotus-features reduce immune responses [13,14]. Attachment and proliferation of fibroblasts, which participate in capsule formation around implanted materials, are inhibited. Simultaneously, competitive cells like human osteoblast-like MG-63 cells are not negatively affected. Additionally, these features control the colonization of pathogenic bacteria (*Staphylococcus aureus* and *Pseudomonas aeruginosa*), which are responsible for risky infections after implantation [12]. However, up to now cell anchorage and osteogenic differentiation in dependence of such lotus-surfaces have not been addressed yet. This was the aim of the following study. The experiments were performed with human adipose-derived stem cells (hASC), which are an attractive cell source in regenerative medicine. In contrast to mesenchymal stem cells from the bone marrow, they are more easily available with higher density and undergo differentiation of various lineages in the same way.

Materials and Methods

Surface structuring, coating and characterization

Pure grade titanium (Ti, Goodfellow, Bad Nauheim, Germany) disks with a diameter of 6 mm were mechanically polished and cleaned with acetone and methanol using an ultrasonic bath. Laser-structuring was performed with an amplified Ti:sapphire femtosecond laser system (Femtopower Compact Pro, Femtolasers Produktions GmbH, Austria), which delivers sub-30 fs laser pulses at 800 nm central wavelength, a pulse energy up to 1 mJ, a repetition rate of 1 kHz. A x-y motorized translation stage (Physik Instrumente GmbH, Germany) was used for sample positioning and translation. Detailed analyses of the material properties with respect to surface roughness via atomic force microscopy and wettability via water contact angle measurements were performed in [12-14]. Finally, the samples were visualized with a scanning electron microscope (SEM). For the *In vitro* studies, the samples were sterilized under UV light for 30 min beforehand. Unstructured and lotus-structured Ti were compared.

Cell culture and seeding onto Ti samples

Unless otherwise noted, chemicals and antibodies were purchased from Sigma-Aldrich (Deisenhofen, Germany), cell culture media and supplements from Lonza (Basel, Switzerland). Human adipose-derived stem cells (hASCs) were isolated and cultured as previously described in [15]. Cells from passages 5-6 were used for the experiments.

Following trypsinization, hASCs were resuspended in control medium Dulbecco`s modified Eagle's medium supplemented with 10% foetal bovine serum (Biochrom AG, Berlin, Germany), 100 U/mL penicillin, and 100 µg/mL streptomycin. They were seeded at a density of 5×10^4 cells/cm² in a medium volume of 500 µL on Ti samples, which were placed on the bottom of 24-multiwell plates. The cells were cultured for 24 h at 37°C in a humidified atmosphere containing 95% air and 5% CO_2. Thereafter, the cell seeded Ti samples were transferred to new 24-multiwell plates in order to discard cells adhered to the plates rather than Ti samples. Osteogenic differentiation was induced with control medium supplemented with 0.1 µM dexamethasone, 10 mM ß-glycerophosphate, and 50 µM ascorbate-2-phosphate for 21 d (referring to osteogenic medium). The media were changed every third day.

On the Ti samples three different cell conditions were compared: (a) control cells cultivated with control medium; (b) differentiated cells cultivated with osteogenic medium – referring to osteogenic cells; and (c) predifferentiated cells, which were differentiated by the usage of osteogenic medium for seven days beforehand, trypsinized, and seeded onto the Ti samples under further osteogenic medium conditions. This setup refers in the following to predifferentiated cells. Then all cell conditions were treated in the same manner.

Cell morphology, proliferation, adhesion, differentiation

The cells were visualized at different time points of cultivation. First, they were observed via SEM (microscope Quanta 400F ESEM (FEI Company, Oregon, USA)). The samples were washed with phosphate buffer saline (PBS) and fixed with 2.5% glutaraldehyde for 15 min followed by 2% osmiumtetroxid for 30 min. Following further washing steps and a dehydration series with different increasing ethanol concentrations, the samples were treated with hexamethyldisilazane. After air-drying the samples were sputter coated with gold for SEM analysis or with silver for energy-dispersive X-ray spectrometry (EDX; EDAX EDS System and Genesis Software, EDAX Inc., New York, USA) analysis. Last was utilized to quantify calcium mineralization via calcium and phosphate as markers for osteogenic differentiation.

Second, after specific stainings, fluorescence images were recorded with Nikon TE-2000 E microscope (Düsseldorf, Germany) and quantified with ImageJ software (http://rsbweb.nih.gov/ij/). Before staining the samples were washed with PBS and fixed in 4% paraformaldehyde for 10 min. Concerning immunofluorescence staining, unspecific antibody binding was inhibited with a 2% bovine serum-PBS solution at 37°C for 30 min. Primary antibodies were diluted in 0.3% Triton X-100 / PBS and incubated at 4°C overnight. After several washing steps, the secondary antibody solution and Hoechst 33342 for nuclei staining were added at 37°C for 1 h.

After 24 h cell viability was determined via calcein AM / ethidium homodimer-1 (Eth-1) staining for viable and dead cells, respectively (Biotium Inc., California, USA). The proliferative activity was detected via Ki67 (Acris Antibodies, Herford, Germany) after 24 h and 7 d. At these time points, all stained cells were counted manually and normalized on the adherent cell number. Last was quantified by counting manually the nuclei on the entire surface. The nuclei were stained with Hoechst 33342. The results were given as average ± standard error of mean (s.e.m) of four independent measurements.

Actin filaments were stained with phalloidin Atto-488 for 20 min. These images were used to quantify cell morphology and orientation like described in [13,16]. The quotient of length and width enabled calculation of cell elongation, which was given as average ± s.e.m. Cells with a ratio smaller than 2 were defined as rounded cells. Their amount was normalized on the entire cell number for each treatment and given in percent. Cells with a ratio bigger than 2 were defined as elongated, and their length was given as average [µm] ± s.e.m. Concerning cell orientation, cell positions within each image were averaged and their corresponding s.e.m. values were calculated. The bigger the s.e.m. value, the less orientated were the cells on the entire surface. All results were obtained from 50 cells per treatment.

Initial cell adhesion events were characterized via α_5 and β_1 integrins (Santa Cruz, Heidelberg, Germany), focal adhesion kinase

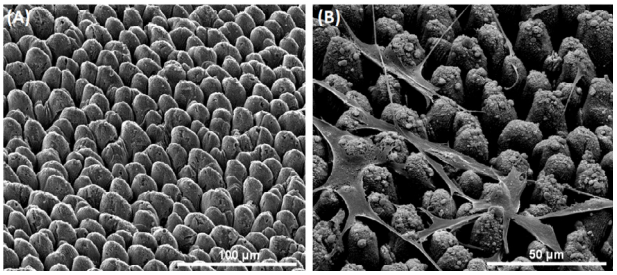

Figure 1: Surface images via electron microscopy (**A**) structured Ti and (**B**) with seeded control hASCs after 24 h.

p-Tyr^{397} (FAK p-Tyr^{397}) and vinculin as components of focal adhesions after 24 h. For quantification a rectangle of 7.5×10^3 pixel^2 was placed on each cell and automatically, the software quantified the mean fluorescence color intensity. A rectangle aside the cells was used as the background signal, which was abstracted from the cell value for each image, separately. The results were given as average ± s.e.m obtained from 50 cells per treatment [16].

Osteogenic differentiation was specified via three specific markers: first, ALP activity of the cells was detected after 7 and 14 d in culture using a histochemical detection with naphthol AS-MX phosphate as a substrate and Fast Red TR salt as coupler; second, osteocalcin expression (Santa Cruz, Heidelberg, Germany) was analyzed after 21 d; third, calcium phosphate deposits were detected via calcein uptake assay after 15 and 21 d in culture. For quantification the fluorescence signals were averaged for each surface type and then normalized on the adherent cell number. The results were given as average of the relative fluorescence intensity ± s.e.m of four independent measurements.

Adhesion force properties

To quantify the anchorage of hASCs to Ti surfaces, detachment force analysis was performed after 24 h and 7 d in culture. According to [17] an engineered rotor construction was utilized, which excludes lateral forces during centrifugation detachment assay. Before and after centrifugation for 10 min with 750 g, the adherent cell number on the samples was determined via the lactate dehydrogenase (LDH) activity. The LDH activity was correlated with the cell number from a cell standard curve prepared in parallel under same conditions (according to the online protocol of OPS DIAGNOSTICS (Lebanon, USA)). Following two washing steps with PBS, 300 µl lysis buffer (1% Triton X-100/PBS) was added. After 30 min incubation time at 37°C, the cell layers and lysis buffer were scraped from samples and transferred to microcentrifuge tubes. After centrifugation at 12000 g for 10 min the supernatants were analyzed via LDH assay; the absorbance was detected at 492 nm wavelength using a microplate reader (Tecan Infinite M200Pro and *Tecan* i-controlTM software, Crailsheim, Germany). The calculated cell density was then used to estimate the parameter Adhesion Force F_{Ad} following the description in [17]. The results were given as average of four independent measurements ± s.e.m.

Statistical analysis

To compare the cell responses Student's-t-test was applied with significance levels of $p<0.05$, $p<0.01$, and $p>0.001$. Thereby, the impact of the topography (*) and differentiation (#) were distinguished.

Results and Discussion

One of the big challenges in biomedical research is devoted to the fabrication of bioactive and osteoinductive biomaterials. Many studies have shown that surface topographies in micro-and nanoscale can significantly control cell behavior, even selectively [18-21]. Nano-materials improved the adhesion and proliferation of osteoblasts and osteoclasts, followed osteogenic differentiation up to 28 d [22]. Proliferation and differentiation of human hipbone primary osteoblasts could be enhanced by nano-topography, whereupon non-periodic nano-features were more effective than nano-tubes or others [23]. Since these studies were performed with osteogenic culture media, the impact of the texturing alone could not be clarified. Others investigated mesenchymal stem cell and osteoprogenitor cell responses to nano-features with different symmetries and degrees of disorder without the usage of osteogenic media [24]. Depending on the surface design, osteogenic differentiation could be triggered, which was also supported by [25]. Micro-scale cavities stimulated the attachment of human osteoblast-like cell line MG-63, but adherent cell number, ALP and osteocalcin expressions were favored on sub-micron scale [26]. Up to now, however, the influences of a lotus-topography, which mimics more accurately the architecture of native bone, have not been addressed yet.

Femtosecond laser irradiation of titanium (Ti) enabled the spontaneous formation of self-organized surface features (Figure 1A). The topography presented microsized convex surface features covered with a nano-roughness similar to lotus leaves (*Nelumbo nucifera*) [12]. From the technical point of view, laser-structuring has many advantages over other technologies such as the controllable and reproducible fabrication of diverse surface features with precise size dimensions in nano- and micro-scale [9-11,13,14]. The usage of ultrashort-pulse lasers minimizes the interaction time between the laser focus and the material, which enables a high resolution, and strongly reduced heat-affected zones. Oxide layers, which support the corrosion resistance of Ti, were also formed on these features [12]. Surface structuring causes an increase of the water contact angle resulting in superhydrophobic surfaces [12]. All produced topographies can additionally be coated [11,21]. Live/dead staining with calcein AM and Eth-1 pointed out that laser-generated Ti surfaces did not cause cytotoxic effects (Figure 1B). We previously reported that laser-structuring of different materials does not induce DNA fragmentation [27]. Since laser ablation of the material does not induce cell death, it can potentially be utilized for biomedical applications [9-11,13,14,21].

On the lotus-topography hASCs adapted their shape to the surface features (Figure 2): the main cell body basically attached on the tip of the microsized texturing, while long cellular extensions were presented in between these features and also rested on neighbouring cells forming a three-dimensional (3D) construct. A comparable 3D network was also described for primary neurons on micro-structures in silicon [28]. It can be concluded that the observed cell alignment on the topography mimics more naturally cell localization *in vivo*. For more insights into surface impacts on cell morphology, cell elongation and orientation were analyzed after 24 h and 13 d (Figure 3 and Table 1). Quantification of day 13 was not possible due to the monolayer on the surfaces.

After 24 h lotus-structures enhanced cell orientation, especially of predifferentiated cells. Control cells were less rounded than predifferentiated cells and presented a significant higher cell ratio and cell length. Moreover, both cell types were more rounded on the flat surface than on the lotus-topography. After 13 d in culture more control and osteogenic cells were adherent on the topography. This observation was supported by quantifying the adherent cell number (Figure 4A). After 24 h the adherent cell number was comparable between unstructured and structured Ti, except for the control cells:

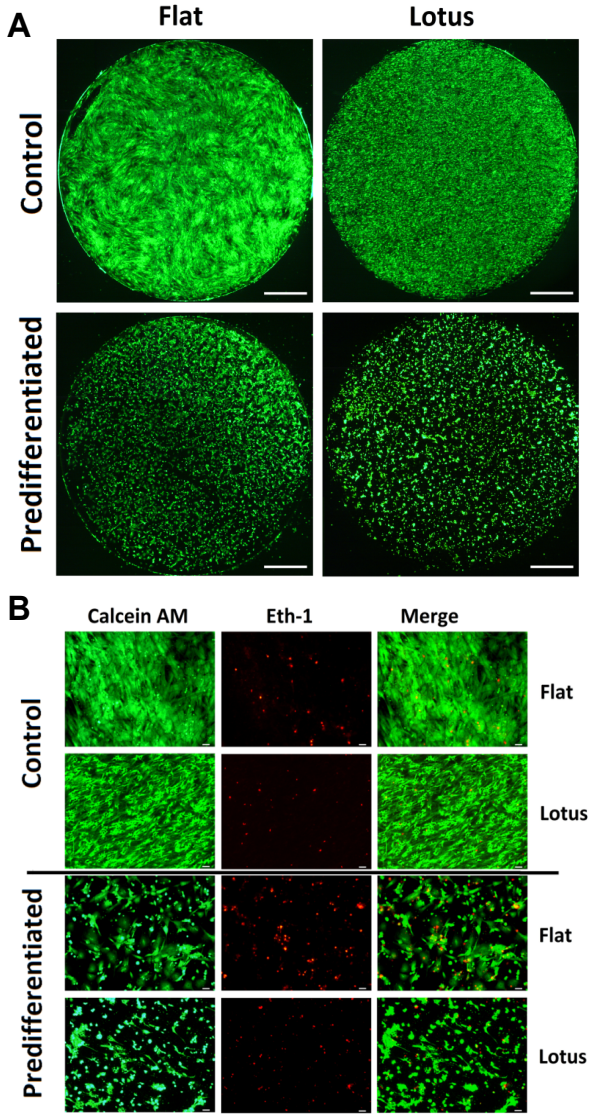

Figure 2: Live/dead staining for the analysis of cell viability after 24 h. Calcein AM stains living cells (green); ethidium homodimer-1 (Eth-1) stains dead cells (red). (A) Overview of the entire sample (scale bars = 1 mm); (B) Detailed view (scale bars = 50 µm).

here, significantly more cells were attached on the laser-generated topography. After longer cultivation times, significantly more control and osteogenic cells were adherent on the lotus-structures. This is due to the increase of surface area and the possible cell alignment in 3D (Figure 1B) [13]. Increase in the adherent cell number correlates with cell proliferation. Basically, the proliferative activity of the cells was higher after 24 h than after 7 d. At both time points, control cells proliferated less than predifferentiated cells (after 24 h) and osteogenic cells (7 d). After longer cultivation times, control cells stopped cell growth, while about 10% of osteogenic cells continued on flat und structured Ti. The reduction of cell growth indicates that the cells may have already switched to osteogenic differentiation. This changeover between proliferation and differentiation is well described for stem cells [8]. Based on this theory it is confusing that osteogenic cells still proliferated after 7 d. We suppose that it was caused by supplements of the osteogenic culture media, namely ascorbic acid. Kaveh et al. [29] described that dexamethasone increases ALP activity, while β-glycerolphosphate stimulates mineralization. However, the role of ascorbic acid on ALP activity is controversial. It was reported that is also facilitates proliferation of mesenchymal stem cells [30]. After 14 d in culture, Ki67 staining revealed that osteogenic and control cells were not proliferative active (Figure not shown).

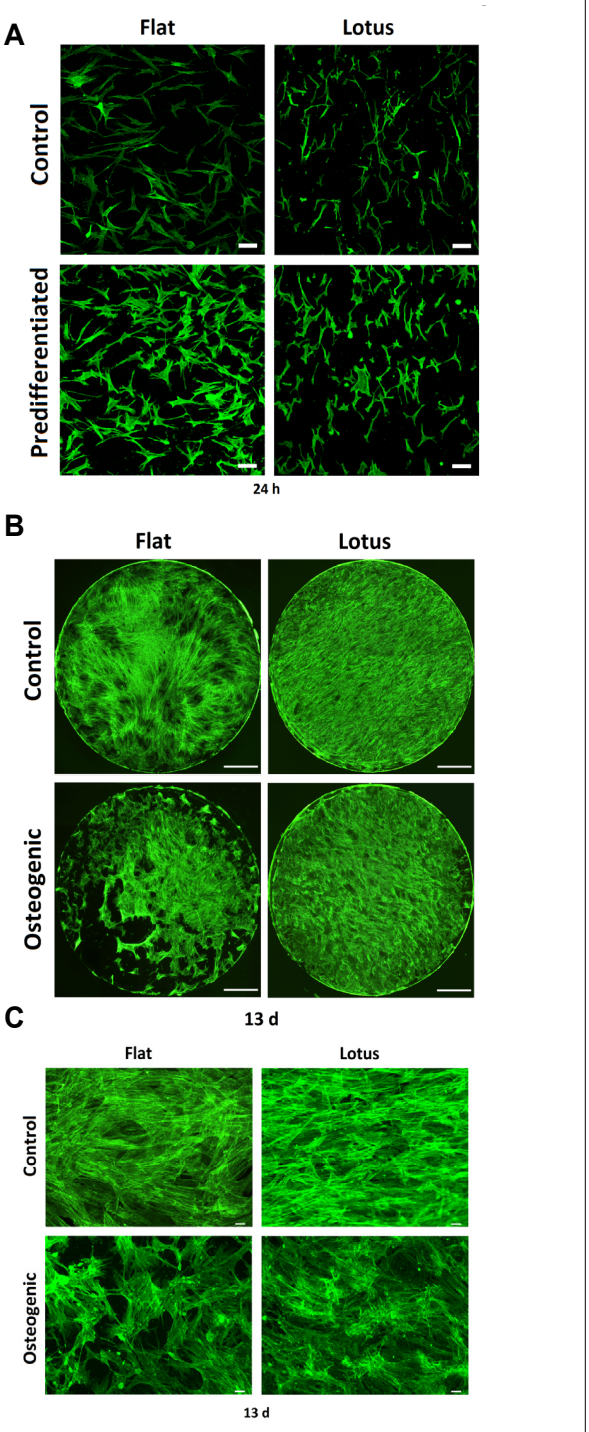

Figure 3: Fluorescence images of stained actin filaments (green) after (A) 24 h (scale bars = 100 µm); and 13 d (B) scale bars = 1 mm and (C) scale bars = 50 µm.

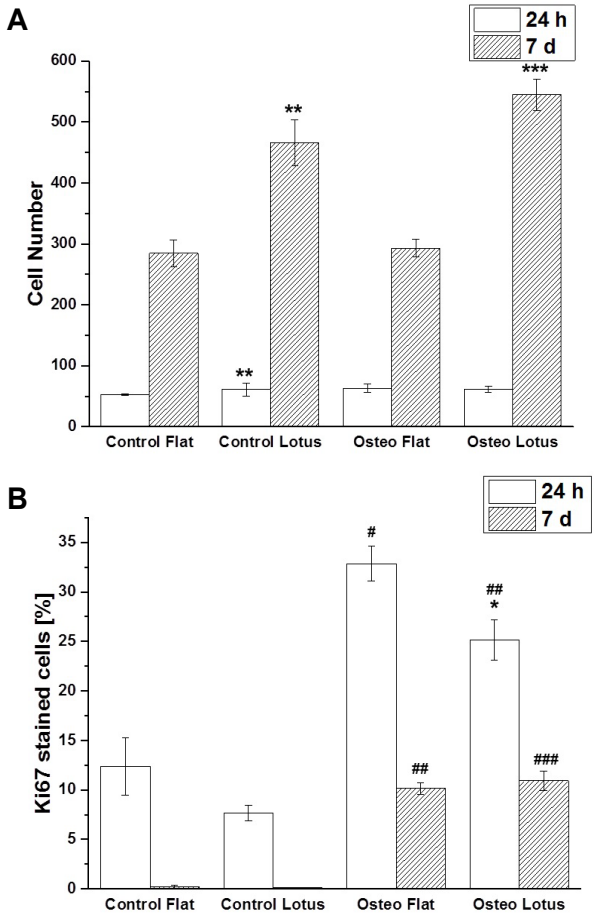

Figure 4: (A) Quantification of adherent cell number on the entire surfaces; (B) analysis of the proliferative activity quantified by the relative amount of Ki67 stained cells. After 24 h control and predifferentiated were compared; after 7 d control and osteogenic cells. Initial cell densities [cells/well] of $2.5x10^4$ and $1x10^5$, respectively. The results are given as average ± s.e.m of four independent measurements. Student's-t-test was applied with significant levels of $p < 0.05$, $p < 0.01$, $p < 0.001$ to compare the impact of the topography (*) and differentiation (#).

Cell	Surface structure	Orientation Angle ± s.e.m.	Cell Ratio [length / width] ± s.e.m.	Amount of rounded cells [%]	Length [µm] ± s.e.m.
Control	Flat	87.54 ± 7.74	4.1 ± 0.23	2	90.85 ± 3.4
	Lotus	90.65 ± 6.28	5.09 ± 0.19 **	0	68.95 ± 3.09 ***
Prediff	Flat	93.07 ± 6.64	2.9 ± 0.14 ###	14	66.72 ± 2.13 ###
	Lotus	95.07 ± 1.36	3.73 ± 0.23 ** ###	8	60.04 ± 1.75 ##

Abbreviations: s.e.m: standard error of mean

Table 1: Quantification of morphology and orientation after 24 h cultivation time. The results are given as average ± s.e.m. of at least 50 cells per treatment. Student's-t-test was applied with significant levels of $p<0.05$, $p<0.01$, $p<0.001$ to compare the impact of the topography (*) and differentiation (#).

Discrepancies in cell morphology of control and osteogenic hASCs may also be due to differentiation differences. Since rounded cells have a limited interaction area with the surface, they are probably not able to build a strong anchorage to the surface. Changes in cell morphology also control stem cell differentiation. It is known that rounded mesenchymal stem cells rather undergo a chondrogenic differentiation, while elongated cells undergo an osteogenic differentiation [31]. These differences depend on actin polymerization and intracellular forces, which are directly linked to the cell shape and adhesion. Both aspects also direct stem cell lineage specification in dependence of material elasticity in a way that stiffer materials promote osteogenic

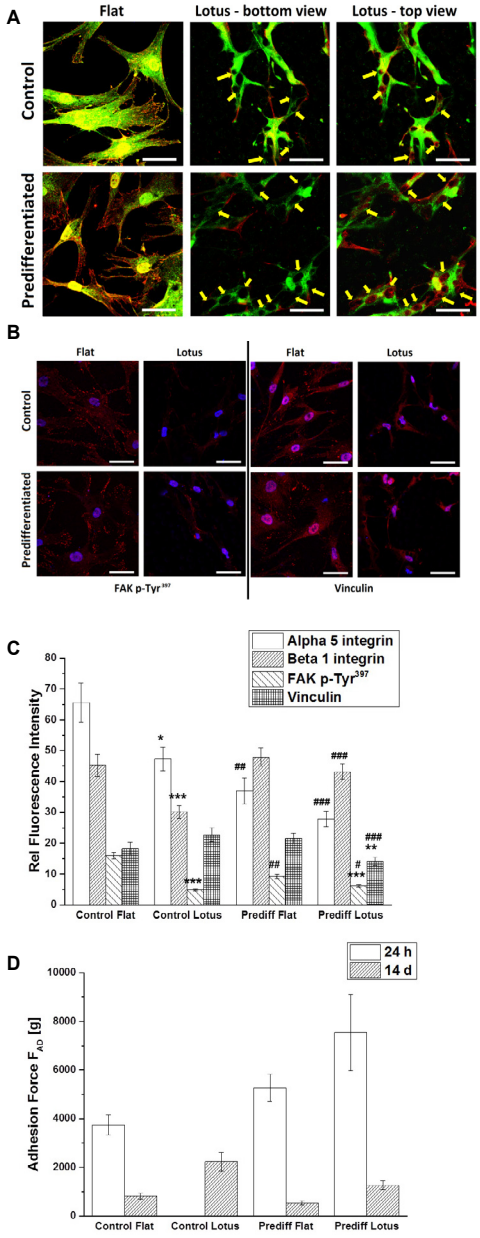

Figure 5: Surface impacts on cell adhesion after 24 h (scale bars = 50 µm). Fluorescence images of (A) α_5 (green) and β_1 (red) integrins (yellow arrows indicate tip of microsized surface features) and of (B) FAK p-Tyr^{397} (red) and vinculin (red) stained cells; nuclei are stained in blue. (C) Quantification of α_5 and β_1 integrins, FAK p-Tyr^{397} and vinculin. The results are given as average ± s.e.m. of at least 50 cells / treatment of four independent measurements. (D) Analysis of adhesion force properties via centrifugation detachment assay after 24 h and 14 d of cultivation. The results are given Adhesion Force F_{Ad} [g] and shown as average ± s.e.m. of obtained of four independent measurements. Student's-t-test was applied with significant levels of $p < 0.05$, $p < 0.01$, $p < 0.001$ to compare the impact of the topography (*) and differentiation (#).

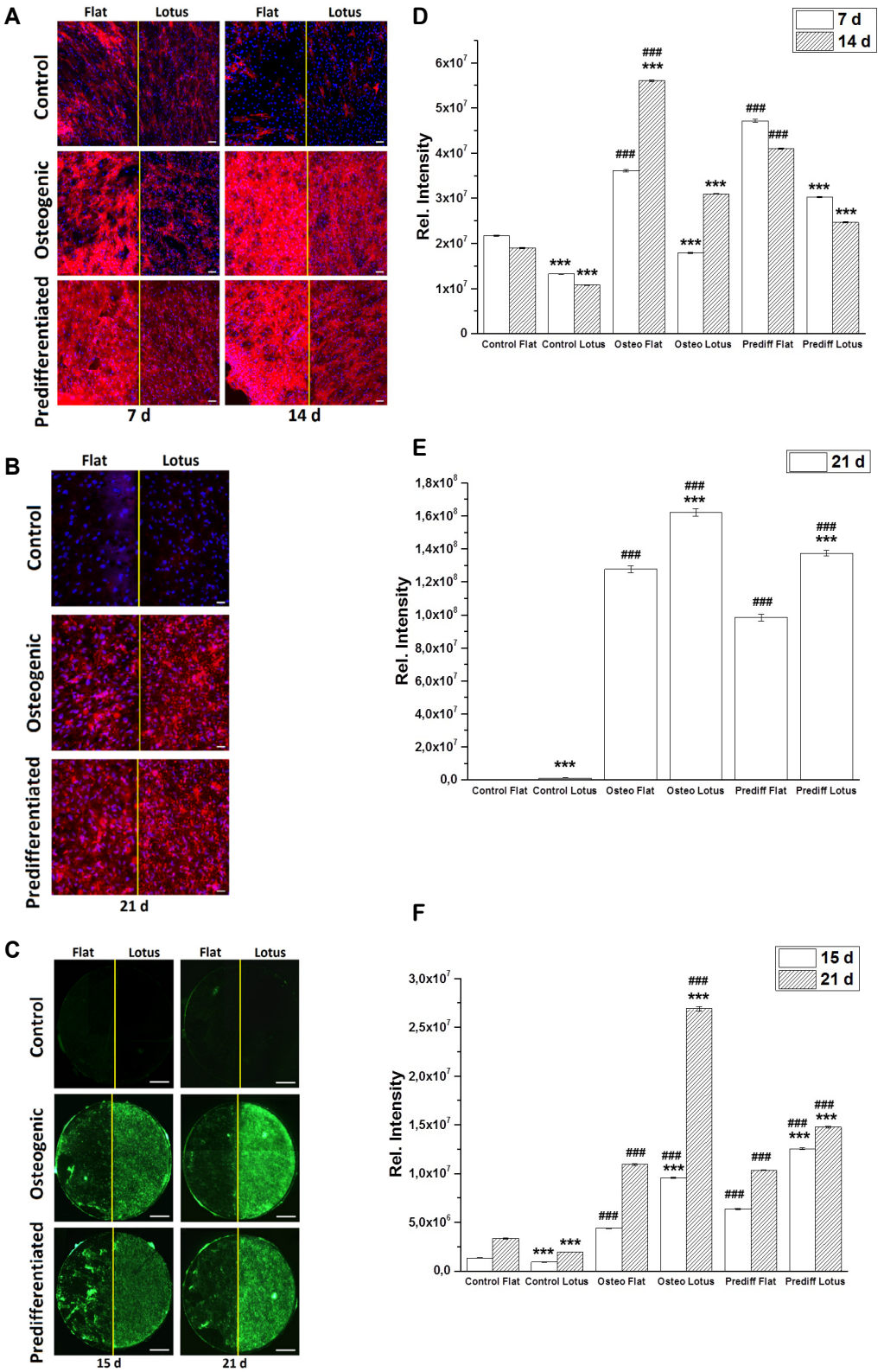

Figure 6: Fluorescence images (A-C) and quantification (D-F) osteogenic markers for control, osteogenic and predifferentiated hASCs. (A, D) ALP activity (red) after 7 and 14 d (scale bars = 100 µm); (B, E) osteocalcin expression (red) after 21 d (scale bars = 100 µm); (C, F) calcein incorporation (green) after 15 and 21 d (scale bars = 1mm). The quantitative results (D-F) are presented as average fluorescence intensity of the entire surface normalized on the adherent cell number ± s.e.m. of obtained of four independent measurements.
Student's-t-test was applied with significant levels of $p < 0.05$, $p < 0.01$, $p < 0.001$ to compare the impact of the topography (*) and differentiation (#).

differentiation [32,33]. The fact that lotus-features in stiff Ti stimulated cell elongation may have a positive outcome on cell anchorage and osteogenic differentiation.

Cell anchorage is not only the key step to induce cell behavior, but also necessary to enhances bone regeneration [1,16]. Thereby, adhesion depends on the binding of the extracellular matrix (ECM), which adsorbs to the material surface, to integrin receptors followed by the formation of focal adhesion complex [34]. Thereafter, signaling cascades are activated to stimulate survival, proliferation and differentiation. The initial adhesion event was characterized after 24 h. On flat Ti α_5 and β_1 integrin subunits were randomly distributed over the entire cell bodies (Figure 5A). In touch with the lotus-topography, this distribution got

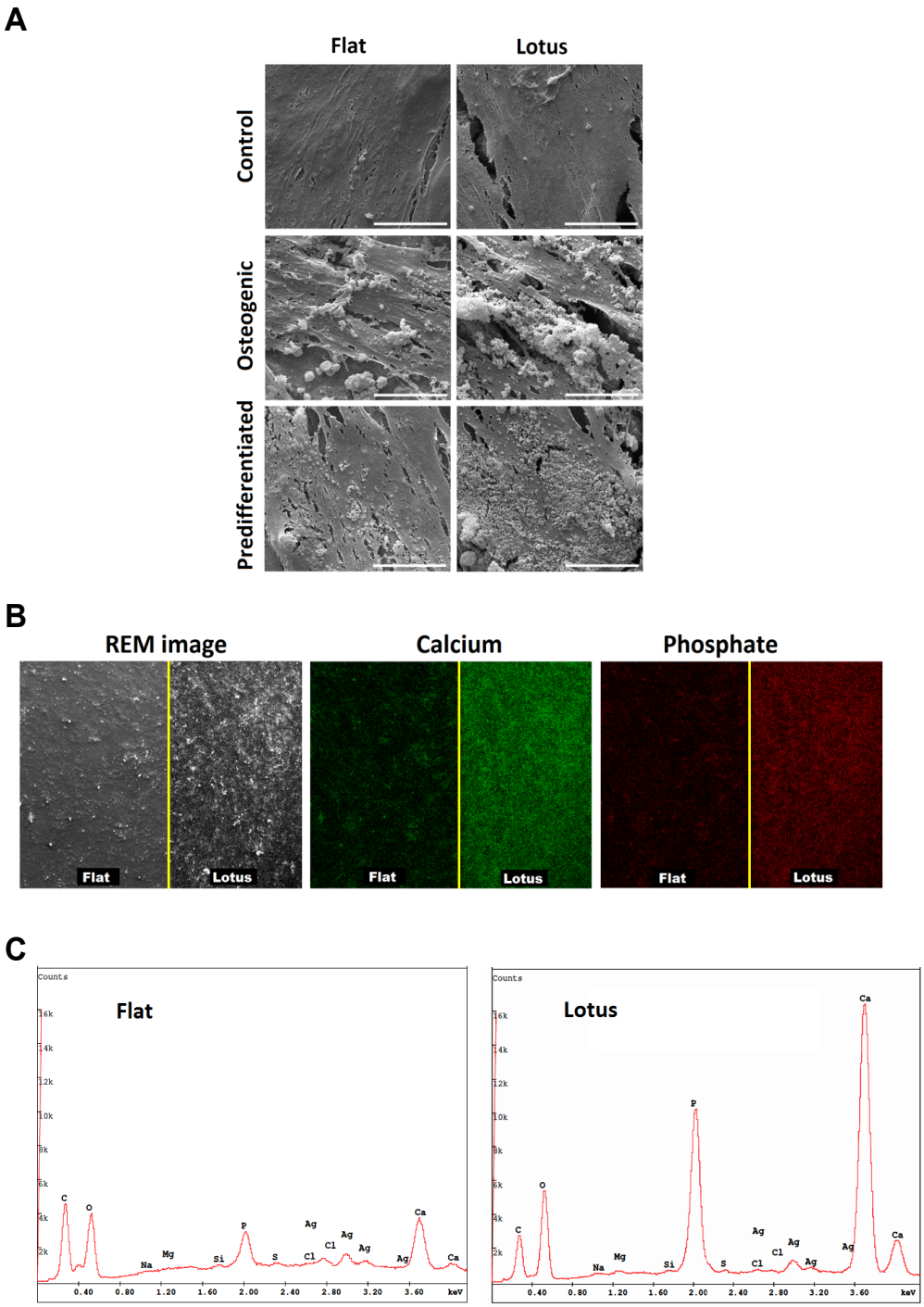

Figure 7: Analysis of calcium mineralization after 21 d. (A) SEM images (scale bars = 20 µm); (B) images used for EDX mapping of osteogenic cells, which show calcium (green) and phosphate (red); (C) corresponding EDX mapping for the detection of calcium and phosphate.

organized: whereas β_1 subunits were basically expressed on the tip of the spikes, α_5 subunits were rather presented at the bottom of the spikes. To our knowledge, this finding has not been described in literature before. Obviously, lotus-structures provide different anchorage points for the cells, which may correlate with a surface specific positioning of ECM binding motives that guide integrin clustering [35].

Additionally, the amount of α_5 and β_1 integrin subunits were quantified. Osteogenic hASC expressed less α_5 subunits than control cells. The observed differences confirm that integrin expression is not constant but varies with the stage of development [36]. Lotus-features reduced significantly α_5 and β_1 levels. Focal adhesion complexes were characterized via focal adhesion kinase p-Tyr^{397} (FAK) and the cytoskeletal component vinculin (Figure 5B). Similar to the integrin results both expression levels were dependent on the differentiation stage. Control cells expressed significantly less FAK than osteogenic cells on unstructured Ti, which was opposite for vinculin. Lotus-structures reduced significantly FAK and vinculin levels (Figure 5C). The functionality of cell anchorage was classified by adhesion force properties at different time points of cultivation (Figure 5D). After 24 h osteogenic cells attached stronger than control cells, after 14 d this was opposite. Generally, cell adhesion forces were lower after longer cultivation times. Lotus-structures significantly improved cell adhesion forces. This result was not expected, since the cytoskeletal component vinculin, which stabilizes focal adhesions, was reduced on the topography. However, since the cells attached in 3D and were more elongated on the lotus-structures (Figures 1B and 3, Table 1), we suppose that they build more binding sites to the structures than we were able to quantify. The discrepancy may correlate with the focus limitation of the imaging system in a way that not all formed binding sites were detectable. In the future, other methods like western blot are necessary to quantify these components. But from the biophysical point of view adhesion forces not only depend on the density of binding sites, but also on the binding distances. If cell attachment to the lotus-structures enables closer binding distances, this may cause stronger cell anchorage effects than the binding density. In Figure 5A surface impacts on integrin subunit localization are shown, which supports this thesis. Further experiments are necessary, to explain this observation. Nevertheless, the adhesion force results point out that this surface design enhances the demanded strong cell anchorage.

Osteogenic differentiation was verified via ALP activity, osteocalcin expression and calcium mineralization at different time points of cultivation (Figures 6 and 7). The results were normalized on the adherent cell number, while all surfaces were totally covered with cells (Figure not shown). In the absence of osteogenic supplements control cells were capable to undergo an osteogenic differentiation to a small extent. However, all markers were significantly higher when osteogenic cell culture medium was added. For *in vivo* applications, it is not a disadvantage that the surface topography alone does not significantly stimulate osteogenic differentiation *in vitro*. All required soluble osteoinductive molecules will be contained within the tissue anyway. Osteogenic predifferentiated cells did not de-differentiate on the surface. Therefore, the surface design may not only be bioactive for osteoprogenitor or stem cells like used here, but also for osteoblasts *in vivo*.

Control cells expressed significantly less ALP than osteogenic and predifferentiated cells (Figures 6A, 6D). Osteogenic cells presented the highest ALP level at 14 d, predifferentiated cells at 7 d. Generally, ALP expression was higher on unstructured Ti. After 21 d control cells were not able to form osteocalcin on unstructured Ti (Figures 6B and 6E). In contact with the lotus-structures, the control cells expressed osteocalcin, even though the amount was significantly lower than for osteogenic and predifferentiated cells. The lotus-topography always increased significantly osteocalcin expression. However, strongest sign for osteoinductive materials is calcium deposition [8]. Calcium mineralization was classified via calcein incorporation (Figures 6C and 6F) and calcium deposition on the surface at different time points (Figure 7A). Osteogenic and predifferentiated cells formed significantly more calcium than control cells. The highest extent was obtained on lotus-structures, especially for osteogenic cells. Electron microscope images further showed cell and surface specific calcium deposits identical to the calcein results (Figure 6A), which were confirmed via EDX analysis (Figures 7B and 7C). It can be concluded that the increase of surface area after lotus-structuring provides a larger contact area for cells and calcium deposits. In a sum, the investigated typical osteogenic markers were selectively affected by the topography: no effect or stimulated. It can be supposed that the osteogenic signaling pathways for these markers differ – and are specifically activated by the topography. Generally, osteogenic differentiation involves interconnected pathways including ERK, p38 and Wnt cascades to stimulate transcription factors like SMAD or RUNX2, which are further regulated by the presence of BMPs and other growth factors [37]. Additionally, it is a question of cell adhesion mechanism, cell shape and intercellular forces. Further basic research is required to explain these observations. However, the differentiation results demonstrated that lotus-structures improved the osteoinductive potential of Ti.

Conclusion

Ultrashort-laser ablation offers the controlled fabrication of various surface designs down to nanoscale. Lotus-structures in titanium, which mimic the hierarchical architecture of native bone, were shown to affect bacteria colonization and inhibit fibrotic scar formation. Here we focussed on the *in vitro* osteoinductive potential using hASCs. Due to the increased surface area for contact, significantly more cells were adherent on the lotus-structures. Interestingly, the distribution of integrin subunits got organized. Furthermore, the structures significantly increased cell adhesion forces. Concerning osteogenic differentiation, the lotus-structures only presented a supportive effect. Analyzing different osteogenic markers, osteocalcin expression and especially calcium mineralization were significantly improved by the structures. Future research is required to understand topographical impacts on the molecular signaling cascades involved in cell adhesion and osteogenic differentiation. Additionally, bioactivity and osseointegration of lotus-structures in Ti have to be investigated *in vivo*.

Acknowledgement

This work was partly supported by the German Research foundation Cluster of Excellence Rebirth “From Regenerative Biology to Reconstructive Therapy” and project “Biofabrication for NIFE”. The authors thank Prof. H. Küster (Leibniz Universität Hannover) for the usage of fluorescence microscope and M. Pflaum (Medical Highschool Hannover) for granting the use of human adipose-derived stem cells. Dr. S. Schlie-Wolter thanks for her scholarship (Habilitation) of the Leibniz Universität of Hannover.

References

1. Geetha M, Singh AK, Asokamani R, Gogia AK (2009) Ti based biomaterials, the ultimate choice for orthopeadic implants – a review. Prog Mater Sci 54: 397-425.
2. Abee T, Kovács AT, Kuipers OP, van der Veen S (2011) Biofilm formation and dispersal in Gram-positive bacteria. Curr Opin Biotechnol 22: 172-179.
3. Anderson JM (2001) Biological responses to materials. Annu Rev Mater Res 31: 81-110.

4. Bosco R, Van den Beucken J, Leeuwenburgh S, Jansen J (2012) Surface engineering for bone implants: a trend from passive to active surfaces. Coatings 2: 95-119.

5. Barrère F, Mahmood TA, de Groot K, Blitterswijk CA (2008) Advanced biomaterials for skeletal tissue regeneration: instructive and smart functions. Mater Scie Eng 59: 38-71.

6. Barradas AM, Yuan H, van Blitterswijk CA, Habibovic P (2011) Osteoinductive biomaterials: current knowledge of properties, experimental models and biological mechanisms. Eur Cell Mater 21: 407-429.

7. Dohan Ehrenfest DM, Coelho PG, Kang BS, Sul YT, Albrektsson T (2010) Classification of osseointegrated implant surfaces: materials, chemistry and topography. Trends Biotechnol 28: 198-206.

8. Birmingham E, Niebur GL, McHugh PE, Shaw G, Barry FP, et al. (2012) Osteogenic differentiation of mesenchymal stem cells is regulated by osteocyte and osteoblast cells in a simplified bone niche. Eur Cell Mater 23: 13-27.

9. Schlie S, Fadeeva E, Koch J, Ngezahayo A, Chichkov BN (2010) Femtosecond laser fabricated spike structures for selective control of cellular behavior. J Biomater Appl 25: 217-233.

10. Schlie S, Fadeeva E, Koroleva A, Chichkov BN (2012) Laser-engineered micro-topography: correlation between structure dimensions and cell control. J Mater Sci: Mater Med 23: 2813-2819.

11. Schlie-Wolter S, Deiwick A, Fadeeva E, Paasche G, Lenarz T, et al. (2013) Topography and coating of platinum improve the electrochemical properties and neuronal guidance. ACS Appl Mater Interfaces 5: 1070-1077.

12. Fadeeva E, Truong VK, Stiesch M, Chichkov BN, Crawford RJ, et al. (2011) Bacterial retention on superhydrophobic titanium surfaces fabricated by femtosecond laser ablation. Langmuir 27: 3012-3019.

13. Fadeeva E, Schlie S, Koch J, Chichkov BN (2010) Selective cell control provided by surface structuring for orthopaedic applications. J Adhes Sci Technol 24: 2257-2270.

14. Schlie S, Fadeeva E, Koroleva A, Ovsianikov A, Koch J, et al. (2011) Laser-based nanoengineering for biomedical applications. Photonic Nanostruct 9: 159-162.

15. Suga H, Shigeura T, Matsumoto D, Inoue K, Kato H, et al. (2007) Rapid expansion of human adipose-derived stromal cells preserving multipotency. Cytotherapy 9: 738-745.

16. Schlie-Wolter S, Ngezahayo A, Chichkov BN (2013) The selective role of ECM components on cell adhesion, morphology, proliferation and communication in vitro. Exp Cell Res 319: 1553-1561.

17. Schlie S, Gruene M, Dittmar H, Chichkov BN (2012) Dynamics of cell attachment: adhesion time and force. Tissue Eng Part C Methods 18: 688-696.

18. Flemming RG, Murphy CJ, Abrams GA, Goodman SL, Nealey PF (1999) Effects of synthetic micro- and nano-structured surfaces on cell behavior. Biomaterials 20: 573-588.

19. Wilkinson CDW, Riehle M, Wood M, Gallagher J, Curtis ASG (2002) The use of materials patterned on a nano- and micro-metric scale in cellular engineering. Mater Sci Eng C 19: 263-269.

20. Bettinger CJ, Langer R, Borenstein JT (2009) Engineering substrate topography at the micro- and nanoscale to control cell function. Angew Chem Int Ed Engl 48: 5406-5415.

21. Fadeeva E, Deiwick A, Chichkov B, Schlie-Wolter S (2014) Impact of laser-structured biomaterial interfaces on guided cell responses. Interface Focus 4: 20130048.

22. Liu H, Webster TJ (2007) Nanomedicine for implants: a review of studies and necessary experimental tools. Biomaterials 28: 354-369.

23. Rani VV, Vinoth-Kumar L, Anitha VC, Manzoor K, Deepthy M, et al. (2012) Osteointegration of titanium implant is sensitive to specific nanostructure morphology. Acta Biomater 8: 1976-1989.

24. Dalby MJ, Gadegaard N, Tare R, Andar A, Riehle MO, et al. (2007) The control of human mesenchymal cell differentiation using nanoscale symmetry and disorder. Nat Mater 6: 997-1003.

25. McNamara LE, McMurray RJ, Biggs MJ, Kantawong F, Oreffo RO, et al. (2010) Nanotopographical control of stem cell differentiation. J Tissue Eng 2010: 120623.

26. Zinger O, Zhao G, Schwartz Z, Simpson J, Wieland M, et al. (2005) Differential regulation of osteoblasts by substrate microstructural features. Biomaterials 26: 1837-1847.

27. Schlie S (2010) Selective cell control for biomedical applications – impact of laser-fabricated 3D scaffolds and surface topographies.

28. Papadopoulou EL, Samara A neuronal web of cytoplasmic processes. Tissue Eng Part C Methods 16: 497-502., Barberoglou M, Manousaki A, Pagakis SN, et al. (2010) Silicon scaffolds promoting three-dimensional

29. Kaveh K, Ibrahim R, Baker ZA, Ibrahim TA (2011) Mesenchymal stem cells, osteogenic lineage and bone tissue engineering: a review. Journal of Animal and Veterinary Advances 10: 2317-2330.

30. Potdar PD, D'Souza SB (2010) Ascorbic acid induces in vitro proliferation of human subcutaneous adipose tissue derived mesenchymal stem cells with upregulation of embryonic stem cell pluripotency markers Oct4 and SOX 2. Hum Cell 23: 152-155.

31. Mathieu PS, Loboa EG (2012) Cytoskeletal and focal adhesion influences on mesenchymal stem cell shape, mechanical properties, and differentiation down osteogenic, adipogenic, and chondrogenic pathways. Tissue Eng Part B Rev 18: 436-444.

32. Engler AJ, Sen S, Sweeney HL, Discher DE (2006) Matrix elasticity directs stem cell lineage specification. Cell 126: 677-689.

33. Evans ND, Minelli C, Gentleman E, LaPointe V, Patankar SN, et al. (2009) Substrate stiffness affects early differentiation events in embryonic stem cells. Eur Cell Mater 18: 1-13.

34. Giancotti FG, Ruoslahti E (1999) Integrin signaling. Science 285: 1028-1032.

35. Cavalcanti-Adam EA, Volberg T, Micoulet A, Kessler H, Geiger B, et al. (2007) Cell spreading and focal adhesion dynamics are regulated by spacing of integrin ligands. Biophys J 92: 2964-2974.

36. Siebers MC, ter Brugge PJ, Walboomers XF, Jansen JA (2005) Integrins as linker proteins between osteoblasts and bone replacing materials. A critical review. Biomaterials 26: 137-146.

37. Kelly DJ, Jacobs CR (2010) The role of mechanical signals in regulating chondrogenesis and osteogenesis of mesenchymal stem cells. Birth Defects Res C Embryo Today 90: 75-85.